Non-Gaussian Features of Transmitted Flux of QSO's Lyα Absorption: Intermittent Exponent

Jesus Pando[1], Long-Long Feng[2,3], Priya Jamkhedkar[4], Wei Zheng[5], David Kirkman[6], David Tytler[6] and Li-Zhi Fang[4]

ABSTRACT

Recently, it has been found that the field traced by QSO's Lyα forests is intermittent on small scales. Intermittent behavior is essential for understanding the statistics and dynamics of cosmic gravitational clustering in the nonlinear regime. The most effective method of describing intermittency uses the structure functions and the intermittent exponent, which measure the scale- and order-dependencies of the ratio between the higher order to second order moments of the field. These properties can be used not only to confirm the non-gaussianity of fields, but also to detect the *type* of non-gaussianity.

In this paper, we calculate the structure function and intermittent exponent of 1.) Keck data, which consists of 28 high resolution, high signal to noise ratio (S/N) QSO Lyα absorption spectra, and 2.) Lyα forest simulation samples produced via the pseudo hydro scheme for the low density cold dark matter (LCDM) model and warm dark matter (WDM) model with particle mass $m_W = 300, 600, 800$ and 1000 eV. Aside from the WDM model with $m_W = 300$ eV, the simulation samples are in agreement with observations in the context of the power spectrum. We find, however, that the intermittent behavior of all the simulation samples is substantially inconsistent, both quantitatively and qualitatively, with the Keck data. Specifically, 1.) the structure functions of the simulation samples are significantly larger than that of Keck data on scales $k \geq 0.1$ km^{-1} s, 2.) the intermittent exponent of the simulation samples is more negative than that of Keck data on all redshifts considered, 3.) the order-dependence of the structure functions of simulation samples are closer to the intermittency of hierarchical clustering on all scales, while the Keck data are closer to a lognormal field on small scales. These differences are independent of noise and show that the intermittent evolution modeled by the pseudo-hydro simulation is substantially different from observations, even though they are in good agreement with each other in terms of second and lower order statistics. This result also shows that "weakly" clustered samples, like high resolution Lyα absorption spectrum, are effective in testing dynamical models of structure formation if their intermittent features are considered.

Subject headings: cosmology: theory - large-scale structure of the universe

1. Introduction

The non-gaussian features of the QSO's Lyα transmitted flux were recently studied and showed that the cosmic mass field traced by the QSO's Lyα forests is intermittent on small scales. That is, the probability distribution functions (PDF) of the transmitted flux fluctuations were found to

[1]Department of Physics, DePaul University, Chicago Il, 60614

[2]Center for Astrophysics, University of Science and Technology of China, Hefei, Anhui 230026,P.R.China

[3]National Astronomical Observatories, Chinese Academy of Science, Chao-Yang District, Beijing, 100012, P.R. China

[4]Department of Physics, University of Arizona, Tucson, AZ 85721

[5]Department of Physics and Astronomy, Johns Hopkins University, MD 21218-2686

[6]Center of Astrophysics and Astronomy, University of California, San Diego, CA 92093

be substantially long tailed on scales less than ~ 1 h^{-1} Mpc. The spatial distribution of the power of the transmission fluctuations was found to be spiky, i.e., the power was concentrated in rare modes while most modes showed very low power (Jamkhedkar, Zhan and Fang 2000; Zhan, Jamkhedkar and Fang 2001; Feng, Pando and Fang 2001).

The impact of intermittency on observational cosmology is that the power spectrum is no longer effective for testing models when intermittency is substantial. Although spikes in the intermittent field are rare and improbable events, one cannot neglect the spikes in measuring the power spectrum as almost all power of the transmission fluctuations is concentrated in these events. In such a case, the power spectrum is dominated by rare and improbable events (spikes). An intermittent field is statistically homogeneous. Yet, the rare events lead to significant differences among samples from different parts of the universe when the spatial size of the region is not large enough to contain numerous spikes. The precision of determining the power spectra is intrinsically constrained by intermittency. The uncertainty of the power spectrum for an intermittent field is inevitably large (Jamkhedkar et al 2002, hereafter Paper I).

Therefore, in the nonlinear regime, more effective measures to compare the predictions of models and observations must be used. Although an intermittent field is non-gaussian, many non-gaussian statistics are ineffective or insensitive to intermittency. This is because we need not only techniques for confirming the non-gaussianity of a field, but also methods which can tell the *type* of non-gaussianity. The most effective measures sensitive to the *type* of intermittency are the structure functions and the intermittent exponent (e.g. Shraiman & Siggia 2000).

In this paper, using a set of 28 high resolution, high signal to noise ratio (S/N) QSO Lyα absorption spectra (Keck data), we will carry out a systematic investigation of the structure functions and the intermittent exponent of the transmitted flux. To show the usefulness of the structure function and intermittent exponent as model discriminators, we also study the intermittent behaviors of Lyα forest samples produced by a pseudo-hydro simulation technique for the LCDM and WDM models. These models are among the best that match the observed power spectrum and other lower than second order statistics. We will show that the simulation samples are significantly intermittent. However, both the quantitative and qualitative properties of simulation samples are found to be substantially different from the Keck data.

The paper is organized as follows. §2 addresses the method for measuring intermittent random fields. §3 presents the algorithm for calculating the structure functions and intermittent exponent. §4 describes, both the observed and simulated samples, that we will use. The power spectrum and other lower order statistics of the Keck data and simulation samples are given in §5. §6 contains the important result, the structure function, intermittent exponent and their of order-, redshift- and scale-dependencies for the Keck data and simulation samples. The emphasis is on revealing the deviation of the intermittent behavior for the simulation samples from the Keck data. Finally, the conclusions and discussions are in §7.

2. Statistical description of an intermittent random field

2.1. Basic properties of an intermittent field

Physically, intermittency is used to characterize a special type of random field in which structures are essentially strong enhancements, peaks or spikes, randomly and widely scattered in space and/or time, with a low field value between the spikes. The spike-gap-spike feature is more pronounced on smaller scales. That is, compared with gaussian fields, the probability distribution function (PDF) of the fluctuations possesses a high peak around zero and possibly a long-tail. The long-tail events correspond to the rare and improbable high peaks. This feature was originally found in the temperature and velocity distributions in turbulence (Batchelor & Townsend 1949).

Mathematically, an intermittent random density field $\rho(x)$ is defined by the ratio between the high- and low-order moments of the field

$$\frac{\langle[\rho(x+r)-\rho(x)]^{2n}\rangle}{[\langle[\rho(x+r)-\rho(x)]^{2}\rangle]^{n}} \asymp \left\langle \frac{r}{L} \right\rangle^{\zeta(n)}, \qquad (1)$$

where L is the size of the sample, and the exponent ζ can be function of n and r. If ζ is negative for small r, the ratio eq.(1) is divergent with $r \rightarrow$

0. This corresponds to an intermittent field. An intermittent field is characterized by the n- and r-dependencies of exponent ζ.

These properties make characterizing intermittent fields by traditional statistical measures difficult. The power spectrum and two-point correlation function are unable to quantify intermittency. Two fields having the same power spectrum may have very different tails in their PDF. Very different from the linear regime, the power spectrum will on longer be a critical discriminator among models of structure formation for an intermittent field.

Equally ineffective are any individual higher order correlation functions and higher order moments of the density fluctuations $\delta(x) = [\rho(x) - \bar{\rho}]/\bar{\rho}$. Three- and four-point correlation functions of the density perturbation $\delta(x)$ are very useful for distinguishing a gaussian from a non-gaussian field. However, they are insensitive to the difference between an intermittent field and a non-gaussian, but non-intermittent field. Moreover, eq.(1) means that the PDF of the density fluctuations $[\rho(x+r) - \rho(x)]$ cannot be expanded into a series of moments of $[\rho(x+r) - \rho(x)]$, as it does not converge. In this case, a better measure is not the divergent quantity itself, $\langle[\rho(x+r) - \rho(x)]^{2n}\rangle/\langle[\rho(x+r) - \rho(x)]^2\rangle^n$ when $r \to 0$, but the quantity describing the divergent behavior, specifically, the exponent ζ.

2.2. Definition of the intermittent exponent

Let us define density difference $\Delta_r(x) \equiv \rho(x+r) - \rho(x)$. The density difference is equal to the density contrast difference, $\delta(x+r) - \delta(x)$, if the mean density $\bar{\rho}$ is normalized to 1. Intermittency is now defined by the divergence of the ratio between the high and low order moments $|\Delta_r(x)|^n$. For a gaussian field, the statistical properties of a field $\rho(x)$ and its difference $\rho(x+r) - \rho(x)$ are the same, while they are different for an intermittent field.

The ensemble average of the moment $|\Delta_r(x)|^{2n}$ is

$$S_r^{2n} = \langle|\Delta_r(x)|^{2n}\rangle \tag{2}$$

where n is a positive integer. If the field is homogeneous, S_r^{2n} is independent of x and depends only on r. S_r^{2n} is called the structure function. When the "fair sample hypothesis" is applicable (Peebles 1980), the structure function can be calculated as the spatial average

$$S_r^{2n} = \frac{1}{L}\int |\Delta_r(x)|^{2n} dx, \tag{3}$$

where L is the spatial range of the sample. When $n = 1$, we have

$$S_r^2 = \langle|\Delta_r(x)|^2\rangle. \tag{4}$$

S_r^2 is the mean of the square of the density fluctuations at wavenumber $k \simeq 2\pi/r$, and therefore, the r-dependence of S_r^2 actually is a different version of the ordinary power spectrum of the field.

The intermittent exponent ζ is defined by[7]

$$\frac{S_r^{2n}}{[S_r^2]^n} \propto \left(\frac{r}{L}\right)^{\zeta}. \tag{5}$$

The intermittency of the field is effectively measured by the structure function and the intermittent exponent.

For an intermittent field, the ratio of S_r^{2n} to $[S_r^2]^n$ is larger for smaller r, and therefore, the exponent ζ is negative. The condition $S_r^{2n} \gg [S_r^2]^n$ on small scales $r \ll L$ indicates that the field contains "abnormal" events of large density fluctuations $|\Delta_r(x)|$ on scale r. Thus, the more negative the exponent ζ on smaller scales, the stronger the "abnormal" events on smaller scales. This gives rise to the spiky structure of an intermittent field. Generally speaking, the intermittent exponent ζ measures the smoothness of the field: for positive ζ, the field is smoother on smaller scales. If ζ is negative, the field is rough on small scales, and can even be singular.

2.3. Examples of the intermittent exponent

1. A Gaussian field.

If the homogeneous and isotropic field is gaussian, the structure function eq.(2) is

$$\begin{aligned} S_r^{2n} &= \int_{-\infty}^{\infty} P_g[\Delta_r(x)]|\Delta_r(x)|^{2n} d\Delta_r(x) \quad (6) \\ &= (2n-1)!!\left[S_r^2\right]^n, \end{aligned}$$

[7] In turbulence, $S_r^{2n}/[S_r^2]^n$ is used to define the so-called anomalous scaling (Shraiman & Siggia 2000.)

where P_g is the gaussian PDF of $\Delta_r(x)$. Thus, if the mass density field is gaussian, we have

$$\frac{S_r^{2n}}{[S_r^2]^n} = (2n-1)!!. \tag{7}$$

This ratio is independent of scale r, and therefore, the intermittent exponent $\zeta = 0$.

2. A self-similar field

For a self-similar field, the average of $\Delta_r(x)$ on different scales satisfies

$$\langle|\Delta_r(x)|^{2n}\rangle = \lambda^{2nh}\langle|\Delta_{\lambda r}(x)|^{2n}\rangle \tag{8}$$

where λ gives the scale factor from r to λr, and h is the self-similar index. In this case, we have

$$S_r^{2n} = \left(\frac{r'}{r}\right)^{2nh} S_{r'}^{2n}, \tag{9}$$

and therefore

$$\frac{S_r^{2n}}{[S_r^2]^n} = \frac{S_{r'}^{2n}}{[S_{r'}^2]^n}. \tag{10}$$

Therefore, $S_r^{2n}/[S_r^2]^n$ is independent of r. We have then $\zeta = 0$ and self-similar fields are not intermittent.

3. Hierarchical clustering.

Hierarchical clustering is popular in modeling the nonlinear clustering of galaxies. This scheme assumes that the correlation functions of the mass density can be described by the linked-pair approximation, i.e., the n-th irreducible correlation function ξ_n is given by the two-point correlation function ξ_2 as $\xi_n = Q_n\xi_2^{n-1}$, where the hierarchical coefficient Q_n is constant (White 1979).

It has been shown that a hierarchical clustered field is (Feng, Pando & Fang 2001)

$$\frac{S_r^{2n}}{[S_r^2]^n} \propto \left(\frac{r}{L}\right)^{-(d-\kappa)(n-1)}, \tag{11}$$

where d is the spatial dimension, and the coefficient κ is a constant depending on the power law index of the power spectrum. In the case where $\kappa < d$, the field is intermittent with exponent

$$\zeta \simeq -(d-\kappa)(n-1). \tag{12}$$

This is the simplest type of intermittency – a mono-fractal with fractal dimension κ in d-dimensional space. A phenomenological model with hierarchical relations was developed by Soneira & Peebles (1977). The model is essentially the same as the so-called β-model of the intermittency in turbulence where a dimension κ fractal distribution in d-dimensional space has the exponent ζ is given by eq.(12) (Frisch 1995.)

4. A Lognormal field

Since the time of Hubble, the lognormal distribution has been used to model the PDFs of the cosmic mass and velocity field, such as the one-point distribution of the number of galaxies, velocity difference, angular momentum, etc (e.g. Yang et al. 2001b). The lognormal model of the baryonic matter distribution (Bi & Davidsen, 1997; Feng & Fang 2000) has also been found to be in good agreement with all observed properties of the Lyα forests.

For a lognormal field, the PDF of $\Delta_r(x)$ is given by

$$P[\Delta_r(x)] = \frac{1}{2^{3/2}\pi^{1/2}|\Delta_r(x)|\sigma(r)} \exp\left\{-\frac{1}{2}\left(\frac{\ln|\Delta_r(x)| - \ln\overline{|\Delta_r(x)|}}{\sigma(r)}\right)^2\right. \tag{13}$$

where the variance $\sigma(r)$ of $\ln|\Delta_r(x)|$ can be a function of the scale r. With eq.(13), we have (Vanmarcke 1983)

$$\frac{S_r^{2n}}{[S_r^2]^n} = e^{2(n^2-n)\sigma^2(r)}. \tag{14}$$

Using eq.(5), the intermittent exponent of a lognormal field is

$$\zeta \simeq 2(n^2-n)\sigma^2(r)/\ln(r/L). \tag{15}$$

When $r < L$, ζ is negative. Therefore, a lognormal field is intermittent.

To summarize, the structure function and intermittent exponent provide a complete and unified description of intermittent fields. The n- and r-dependencies of the structure functions and intermittent exponent ζ are sensitive to the details of the intermittency of the field. These measures are very powerful for distinguishing among fields that are gaussian, self-similar, mono-fractal, multi-fractal, and singular.

3. The intermittent exponent

3.1. Statistical variables in the DWT representation

The quantity $\Delta_r(x)$ or $[\delta(x+r)-\delta(x)]$ contains two variables: the position x and the scale r, and therefore, $\delta(x)-\delta(x+r)$ should be calculated with a space-scale decomposition. Moreover, as defined by eq.(2), S_r^{2n} is sometimes a diverging quantity. For instance, $\langle S_r^2\rangle = 2[\langle\delta(x)\delta(x)\rangle - \langle\delta(x)\delta(x+r)\rangle]$ is divergent if the 2-point correlation function $\langle\delta(x)\delta(x+r)\rangle \simeq r^{-\alpha}$. This problem can be handled in the same way as N-point correlation functions are handled, i.e., smoothing the density field at small scale prior to its measurement. However, the size of the smoothing scale is put in by hand and might induce uncertainties, especially in studying the scaling behavior on scale comparable with the smoothing size.

Ideally one would like a space-scale decomposition without the need for pre–smoothing by hand. This leads us to chose the discrete wavelet transform (DWT). The DWT performs a smoothing "automatically" as the density difference $[\delta(x) - \delta(x+r)]$ on scale r is calculated by a difference between the smoothed densities at spatial ranges $(x, x+r/2)$ and $(x+r/2, x+r)$. In wavelet analysis, the smoothing is done scale-by-scale. Moreover, the bases that the DWT uses for smoothing and decomposing distributions are orthogonal and complete. The smoothing and decomposition are optimized and there is no loss of information. Furthermore, no mixing of the density fluctuations among different scales occurs. This property is excellent for studying scaling.

Here we only very briefly introduce the DWT decomposition, as it has been introduced in our previous publications (e.g. Pando & Fang 1996; Pando & Fang 1998; Fang & Feng 2000). For details on the DWT refer to Mallat (1989a,b); Meyer (1992); Daubechies, (1992), and for physical applications, refer to Fang & Thews (1998).

We restrict our discussion to a 1-D random field of the transmission flux $F(x)$ extending in a spatial or redshift range $L = x_2 - x_1$. To apply the DWT, we first chop the spatial range $L = x_2 - x_1$ of the 1-D sample into 2^j subintervals labeled with $l = 0, ...2^j - 1$ where j is a positive integer. Each subinterval spans a spatial range $L/2^j$. The subinterval l is from $x_1 + Ll/2^j$ to $x_1 + L(l+1)/2^j$. That is, we decompose the space L into cells (j, l), where j denotes the scale $L/2^j$, and l the spatial range $(x_1 + Ll/2^j, x_1 + L(l+1)/2^j)$. Cell (j, l) is localized in scale space and physical (or redshift) space.

Corresponding to each cell, there is a scaling function $\phi_{j,l}(x)$, and a wavelet function $\psi_{j,l}(x)$. These functions are the basis for the scale-space decomposition. The most important property of the DWT basis is its locality in both scale and physical spaces. The scaling function $\phi_{j,l}(x)$ is a window function on scale j and at position l. The wavelet function $\psi_{jl}(x)$ is admissible (Daubechies 1992), i.e., $\int \psi_{jl}(x)dx = 0$, and therefore, it measures the fluctuation on scale j and at position l.

With the DWT, a transmission $F(x)$ can be decomposed as (Fang & Thews 1998).

$$F(x) = \sum_{l=0}^{2^j-1} \epsilon^F_{j,l}\phi_{jl}(x) + \sum_{j'=j}^{J}\sum_{l=0}^{2^{j'}-1} \tilde{\epsilon}^F_{j',l}\psi_{j',l}(x), \tag{16}$$

where J is given by the finest scale (resolution) of the sample, i.e., $\Delta z = L/2^J$, and j is the scale of interest. The scaling function coefficient (SFC) ϵ^F_{jl} in eq.(16) is given by projecting $F(x)$ onto $\phi_{j,l}(x)$

$$\epsilon^F_{j,l} = \int F(x)\phi_{j,l}(x)dx. \tag{17}$$

The SFC $\epsilon^F_{j,l}$ describes the mean (or smoothed) field of the mode (j, l).

The wavelet function coefficient (WFC), $\tilde{\epsilon}^F_{j,l}$, in eq.(16) is obtained by projecting $F(x)$ onto $\psi_{j,l}(x)$

$$\tilde{\epsilon}^F_{j,l} = \int F(x)\psi_{j,l}(x)dx. \tag{18}$$

The WFC is basically the difference between the smoothed flux $F(x)$ in cells $[x_1 + lL/2^j, x_1 + (l + 1/2)L/2^j]$ and $[x_1+(l+1/2)L/2^j, x_1+(l+1)L/2^j]$. Therefore, the WFC $\tilde{\epsilon}^F_{j,l}$ can be used as the variable $\delta(x+r)-\delta(x)$ in §2, where $x \simeq x_1+lL/2^j$ and $r \simeq L/2^j$. All compactly supported wavelet bases produce similar results. We will use Daubechies 4 in the study below.

3.2. The intermittent exponent in the DWT basis

We can express eq.(3) in the DWT representation by replacing the density difference, $\delta(x+r)-$

$\delta(x)$, by the wavelet coefficient $\tilde{\epsilon}^F_{j,l}$ as discussed in §3.1. Thus,

$$S_j^{2n} = \langle |\tilde{\epsilon}_{j,l}|^{2n} \rangle = \frac{1}{2^j} \sum_{l=0}^{2^j-1} |\tilde{\epsilon}^F_{j,l}|^{2n}, \qquad (19)$$

where j plays the same role as r in eq.(3). S_j^{2n} is the mean of moment $|\tilde{\epsilon}^F_{j,l}|^{2n}$ over the position index l. With the DWT, eq.(4) becomes

$$S_j^2 = \frac{1}{2^j} \sum_{l=0}^{2^j-1} |\tilde{\epsilon}^F_{j,l}|^2. \qquad (20)$$

In Paper I, S_j^2 is used to define the DWT power spectrum P_j^u, i.e. $P_j^u = S_j^2$. P_j^u is the power spectrum of the transmitted flux fluctuations $\Delta F = F - \langle F \rangle$. In Paper I, or Jamkhedkar, Bi & Fang (2001), and Yang et al. (2001a), the power spectrum P_j^u differs from eq.(20) and (21) by a noise term. Since the noise is gaussian, this term can be ignored on scales for which S_j^2 is larger than the variance of the noise.

Eq.(20) can also be written as $S_j^2 = \frac{1}{2^j} \sum_{l=0}^{2^j-1} P^u_{jl}$, where

$$P^u_{jl} = |\tilde{\epsilon}^F_{j,l}|^2 \qquad (21)$$

where P^u_{jl} is the local power, i.e., the power on scale j at position l.

Considering $r \simeq L/2^j$, the intermittent exponent ζ [eq.(5)] can be calculated from

$$\frac{S_j^{2n}}{[S_j^2]^n} \propto 2^{-j\zeta}. \qquad (22)$$

Generally, ζ depends on n and j.

4. Samples

4.1. Keck data of Lyα forests

The experimental data used in our study is the same as Paper I. It consists of 28 Keck HIRES QSO spectra (Kirkman & Tytler 1997). The QSO emission redshifts cover a redshift range from 2.19 to 4.11. For each of the 28 QSO's, the data are given in terms of pixels with wavelength λ_i, flux $F(\lambda_i)$ and noise $\sigma(\lambda_i)$. The noise includes the Poisson fluctuations and the noise due to the background and the instrumentation. The continuum of each spectrum is given by IRAF CONTINUUM fitting.

For our purposes, the useful wavelength region is from the Lyβ emission to the Lyα emission, excluding a region of about 0.06 in redshift close to the quasar to avoid any proximity effects. In this wavelength range, the number of pixels is about 1.2×10^4 for each spectrum.

For all bins in this data set, the ratio $\Delta\lambda/\lambda$ is constant, $\Delta\lambda/\lambda \simeq 13.8 \times 10^{-6}$, or $\delta v \simeq 4.01$ km s^{-1}, and therefore, the resolution is about 8 km s^{-1}. The distance between N pixels in units of the local velocity scale is given by $\Delta v = 2c(1 - \exp[-(1/2)N\delta v/c])$ km s^{-1}, or wavenumber $k = 2\pi/\Delta v$ km^{-1} s.

We do a scale by scale decomposition of the data. We use only $2^{13} = 8192$ pixels for each spectrum. Thus, each cell on scale j corresponds to $N = 2^{13-j}$ pixels. The smallest scales are generally dominated by noise. We study only scales $\geq$ 16 km s^{-1}, corresponding to ≥ 4 pixels or $j \leq 11$, and $k \leq 0.4$ km^{-1} s. Since metal lines are generally narrow with Doppler parameter b$<$ 15 km s^{-1}, ignoring scales less than 16 km s^{-1} also suppresses metal line contamination. The algorithm for treating unwanted data (pixels with negative flux or missing data) and detected metal lines with space-scale decomposition will be discussed in more detail in §4.3.

In applying our algorithm, we sometimes use the 28 QSO transmissions individually, i.e. calculate the statistics of the transmission over each QSO separately, and sometimes all the transmissions are treated together. In the latter case, we divide the data into 12 redshift ranges from $z = 1.6 + n \times 0.20$ to $1.6 + (n+1) \times 0.20$ where $n = 0, 1, ..11$. All the transmission flux in a given redshift range forms an ensemble. Note that the number of data points in each redshift range is different.

4.2. Simulation samples

The simulated samples of the Lyα forests are produced as in Paper I. Besides the LCDM model, we also simulate the warm dark matter (WDM) model, for which the linear power spectrum on scales smaller than the free-streaming length of the warm particle, $R_f = 0.2(\Omega_0 h^2)^{1/3}(m_W/\mathrm{keV})^{-4/3}$, is damped exponentially with respect to the pure CDM model.

The WDM model is believed to be a possible

candidate to solve the problem of cuspy halos, or the singular mass profiles of massive objects. The problem appears in high resolution N-body simulations of CDM models where the models predict central cusps in the dark halos (Jing & Suto 2000). However, observations instead show soft halo profiles as inferred from low surface brightness galaxies and the rotation curves of dwarf galaxies (Flores & Primack 1994, Burkeret 1995). The WDM models are able to soften the density profile of the central core, while at the same time having no effect on large scales. Hence, WDM models are proposed in order to deal with the nonlinear clustering on small scales. Since the cosmic field on those scales is already intermittent, it is important to examine the intermittent behavior of the WDM models. We consider four WDM models having particle masses $m_W = 300, 600, 800$ and 1000 eV.

4.3. Treatment of unwanted data

In the Keck transmission flux, there are suspect data including bad pixels (gaps without data), and negative flux pixels. The latter are generally saturated absorption regions having lower S/N. Although the percentage of low S/N data is not large, it will introduce large uncertainties in the analysis.

As in Paper I, we use the conditional-counting method to treat the unwanted data. Briefly, the algorithm is as follows:

1. Calculate the SFCs for both the transmission $F(\lambda)$ and noise $\sigma(\lambda)$, i.e.
$$\epsilon^F_{jl} = \int F(x)\phi_{jl}(x)dx, \quad \epsilon^N_{jl} = \int \sigma(x)\phi_{jl}(x)dx. \tag{23}$$
2. Identify unwanted mode (j, l) using the condition
$$\left|\frac{\epsilon^F_{jl}}{\epsilon^N_{jl}}\right| < f \tag{24}$$
where f is a constant. This condition flags all modes with S/N less than f. We can also flag modes dominated by metal lines.
3. Since all the statistical quantities in the DWT representation are based on an average over the modes (j, l), we do not count all the flagged modes when computing these averages.

Condition (24) is applied at each scale j. If the size of a bad data segment is d, condition (24) only flags modes (j, l) on scales less than or comparable to d. Therefore in this algorithm, no rejoining and smoothing of the data is needed. We also flag two modes around a unwanted mode to reduce any boundary effects of the chunks. With this method, we can still calculate the structure functions and intermittent exponent by eqs.(19), (20) and (22), but the average is not over all modes, but over the un-flagged modes only. Since the DWT calculation assumes the sample is periodized, this may cause uncertainty at the boundary. To reduce this effect, we drop 5 modes near the boundary.

5. Second and lower order statistical properties

5.1. The power spectrum

The power spectra of the transmitted flux of the Keck data and simulated LCDM samples have been studied in detail in Paper I. The spatial distribution of local power P^u_{jl} show spiky features. This property leads to large uncertainty of P^u_j.

Now we do a similar analysis for the WDM samples. Fig. 1 plots the mean and error bars for P^u_j for $j = 10$ ($k = 0.2$ km^{-1} s) of the 28 QSO's pseudo hydro simulation samples for the WDM model with $m_W = 300, 600, 800$ and 1000 eV. For each QSO, we calculate the mean P^u_j for each realization then calculate the mean over the 20 realizations. The error bar is given by the range of P^u_js by dropping the highest and lowest P^u_j of the 20 realizations. This is equivalent to dropping the top and bottom 5% of the data. As expected, the mean power P^u_j is slightly lower for smaller m_W. But the error bars of the power spectrum are generally much larger than the m_W-dependence of P^u_j.

In Fig. 2, we present the mean of the power spectrum in 8 redshift bins and on scales $j = 8$ to 11 ($k = 0.05, 0.1, 0.2, 0.4$ km^{-1} s) for the Keck data and all the simulated samples. On scale $j = 8$ ($k = 0.05$ km^{-1} s) and for all redshift bins, the powers decrease in the order from LCDM, to the WDM of $m_W = 1000$, 800, 600, and 300 eV. This order is expected, as on scale $j = 8$ and redshift $z > 2$, the nonlinear and intermittent features are weak, and the power spectra trends are about the same as in linear regime. That is the power is

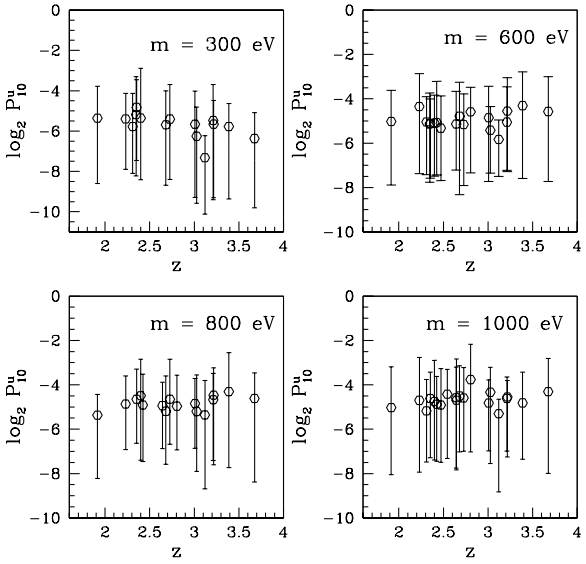

Fig. 1.— The power, P_j^u, on scale $j = 10$ ($k = 0.2$ km^{-1} s) of the 28 QSO's pseudo hydro simulated samples for the WDM models $m_W = 300, 600, 800$ and 1000 eV. The mean is given by average the of the power of the 20 realizations for each QSOs. The error bars are the dispersion of 18 realizations, which are given by dropping the highest and lowest P_j^u of the 20 realizations.

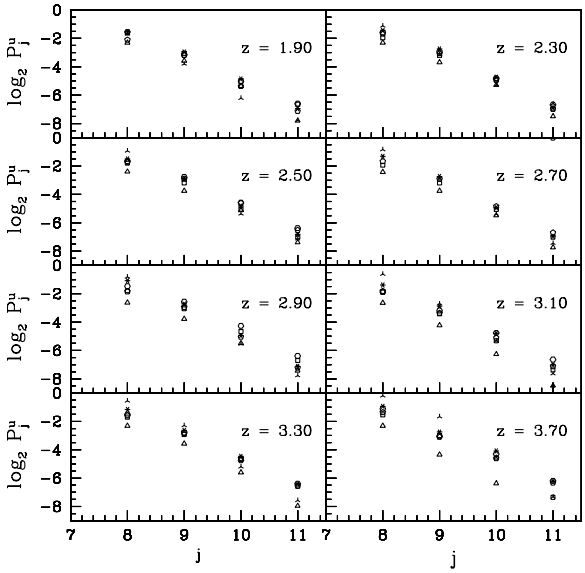

Fig. 2.— The power spectrum P_j^u vs. j for Keck data (vertex with three legs), LCDM (vertex with six legs) and WDM models of m_W= 1000 (hexagon), 800 (pentagon), 600 (square) and 300 (triangle) eV. in redshift bins 1.90 ± 0.1, 2.3 ± 0.1, 2.5 ± 0.1, 2.7 ± 0.1, 2.9 ± 0.1, 3.1 ± 0.1, 3.3 ± 0.1 and 3.7 ± 0.1. The wavenumber for scale j is $k = 0.4 \times 2^{j-11}$ km^{-1} s.

smaller for smaller m_W, and the LCDM corresponds to an infinite mass m_W. On scales $j > 8$ ($k > 0.05$ km^{-1} s) the trend changes. This is because the nonlinear evolution is significant on these scales. The mean power is mainly dependent on rare and improbable events, and therefore, it induces a large uncertainty.

Fig. 2 also shows that the power spectrum of the WDM model with $m_W = 300$ eV is systematically lower than the power of Keck data on almost all scales and higher redshifts ($z > 2.3$). Therefore, this model can be ruled out by the power spectrum. On the other hand, there are no systematic differences between the power spectra of the real data, and the LCDM, or WDM ($m_W = 600, 800, 1000$eV) data. The dispersions among these power spectra generally are less than a factor of 2. Considering the error bars of the observed power spectrum (Paper I) and that shown in Fig. 1 are larger than by a factor of 2, the LCDM, $m_W = 1000, 800$ and 600 eV models are basically consistent with the Keck data. This

is one reason for proposing WDM models with $m_W > 600$ eV.

5.2. Cumulative distribution function (CDF) of local powers

The PDF of the local power P^u_{jl} [eq.(21)] for a given j are found to be long tailed (Paper I). This property can also be shown by the cumulative distribution function (CDF), which is defined as the percentage of the modes with local power less than a given P^u_{jl}/P^u_j. Fig. 3 presents the CDFs of P^u_{jl}/P^u_j on scales $j = 8, 9, 10$ and 11 ($k = 0.05, 0.1, 0.2, 0.4$ km^{-1} s), and in redshift range 1.7 to 1.9.

The CDFs generally consist of two parts: a rapidly growing branch at $P^u_{jl}/P^u_j < 1$, and very slowly growing branch at $P^u_{jl}/P^u_j \gg 1$. The latter is given by spiky modes and the former from the passive modes between the spikes.

For a gaussian field, the PDF of P^u_{jl} is a $\chi^2(N = 1)$ distribution. The CDF of the χ^2 distribution is also shown in Fig. 3 (dotted line). This CDF approaches 1 at $P^u_{jl}/P^u_j \simeq 10$, i.e. $\sim 3\ \sigma$. Fig. 3 shows that the CDF of the Keck data approaches 1 at $P^u_{jl}/P^u_j \simeq 15$ ($j = 8$), 20 ($j = 9$), 30 ($j = 10$), and 60 ($j = 11$) and shows that the Keck's CDF on small scales has a much longer tail than a gaussian field.

We also calculate the CDFs of the quasi-hydro simulation samples for the LCDM and WDM models. The CDFs of simulation samples are generally in good agreement with the Keck data. Only the CDF of model $m_W = 300$ eV on scale $j = 8$ shows a strong deviation from Keck data at $P^u_{jl}/P^u_j \geq 5$.

On scales $j = 10$ and 11, the CDFs of the simulation samples show a little more rapid growth at $P^u_{jl}/P^u_j < 1$ than Keck data, and longer tail than the Keck data at $P^u_{jl}/P^u_j > 10$. The CDF of the simulation samples approaches 1 at $P^u_{jl}/P^u_j \simeq 60$ ($j = 10$), and 100 ($j = 11$). This seems to indicate that the long tail behavior of the quasi-hydro simulation samples is more prominent than the observed samples.

However, care should be taken about any conclusion made with the CDFs. The rapidly growing branch, which is given by the quiet modes, is sensitive to noise. On the other hand, the horizontal branch is sensitive to spiky events, and therefore, depends on the number of modes of the sample

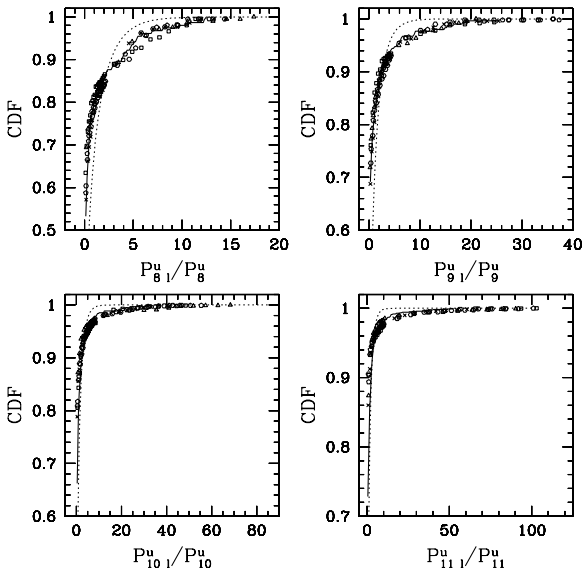

Fig. 3.— The CDF of P^u_{jl}/P^u_j on scales $j = 8, 9, 10$ and 11 for Keck data (solid line), LCDM (cross), and WDM models of m_W= 1000 (hexagon), 800 (pentagon), 600 (square) and 300 (triangle) eV in redshift bins 1.90 ± 0.1. The dotted lines are for gaussian field, i.e. the CDF of $\chi^2(N = 1)$ distribution. The wavenumber for scale j is $k = 0.4 \times 2^{j-11}$ km^{-1} s.

considered. Therefore, from the CDFs of Fig. 3, one can only conclude that the LCDM and WDM with $m_W = 600$, 800, and 1000 eV are consistent with the Keck data.

5.3. Probability distribution functions of the SFCs

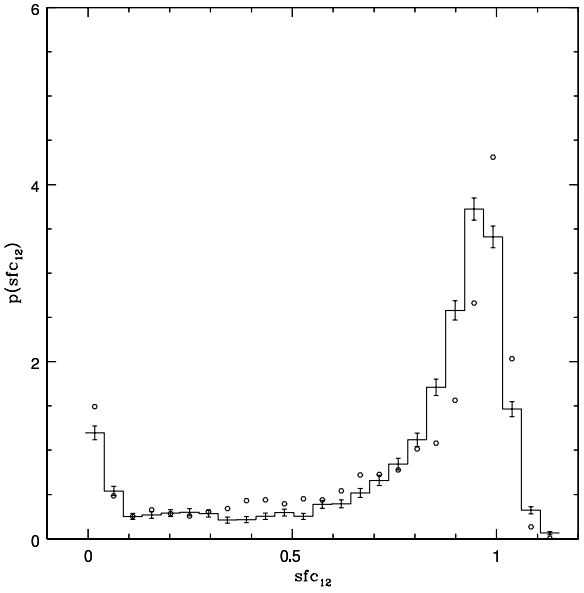

Fig. 4.— The PDF of flux $\sqrt{2^j/L}\epsilon^F_{jl}$ on scales $j = 12$ for observed (histogram) and simulated LCDM samples (circular) of Q0130 on scales $j = 12$ ($k = 0.8$ km^{-1} s). The redshift of the transmitted flux is in the ranges $z = 2.4$ - 2.6. The error bars are given by bootstrap resampling.

The PDF of the transmitted flux F is often used as a statistical measure of the Lyα forests. The SFCs ϵ^F_{jl} defined by eq.(17) are proportional to the Lyα transmitted flux at position l. The ϵ^F_{jl} multiplied by $\sqrt{2^j/L}$ is the mean transmitted flux in the cell (j, l). Therefore, the PDF of $\sqrt{2^j/L}\epsilon^F_{jl}$ is the PDF of F smoothed on scale j.

As an example, Fig. 4 presents the PDF of $\sqrt{2^j/L}\epsilon^F_{jl}$ for the observed QSO, Q0131 on scales $j = 12$. The error bars are given by bootstrap resampling. In Fig. 4, we also plot the PDFs of $\sqrt{2^j/L}\epsilon^F_{jl}$ on $j = 12$ ($k = 0.8$ km^{-1} s) for a simulation sample of the LCDM model. It can be seen, even on this small scale, that the PDFs of the simulation sample basically are still consistent with observations. The biggest difference between the observation and model prediction is at $\sqrt{2^j/L}\epsilon^F_{jl} \simeq 1$. However, this difference is sensitive to noise. Fig. 5 gives the PDFs of $\sqrt{2^j/L}\epsilon^F_{jl}$ on $j = 10$ ($k = 0.2$ km^{-1} s) for the LCDM simulation, but with gaussian noise of different σ added. The peak at $\sqrt{2^j/L}\epsilon^F_{jl} \simeq 1$ is significantly dependent on the noise. Moreover, for the Keck sample, the noise level is correlated with F. Generally, noise is high at $F \simeq 1$, and low at $F \simeq 0$. This makes the peak of the PDF at $\sqrt{2^j/L}\epsilon^F_{jl} \simeq 1$ more uncertain.

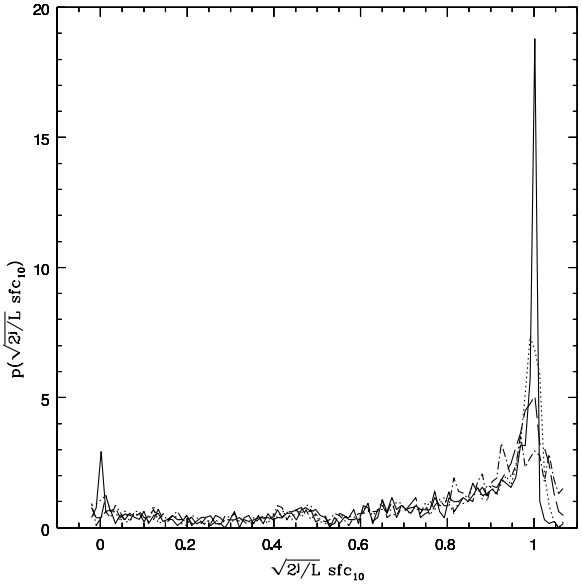

Fig. 5.— The PDF of SFCs $\sqrt{2^j/L}\epsilon^F_{jl}$ scales $j = 10$ ($k = 0.2$ km^{-1} s) for simulated LCDM samples for Q0130. The samples are added gaussian noise in each bin with standard deviation zero (solid), σ (dot), 2σ (dash), and 4σ (dot-dash), where σ is the mean standard deviation for the keck samples.

Statistics with SFCs ϵ^F_{jl} [eq.(17)] generally are more sensitive to noise than WFCs $\tilde{\epsilon}^F_{j,l}$ [eq.(18)]. This is because $\tilde{\epsilon}^F_{j,l}$ is the density *difference* between neighboring positions, and the uncertainty of the background noise on large scales is canceled in this difference. On the other hand, ϵ^F_{jl} is the mean density at l, it is contaminated by the uncertainty of the background noise on all large scales. Thus, one may conclude that the PDFs of flux F is not reliable as a discriminator.

6. Structure functions and intermittent exponent of Lyα forests

6.1. Structure functions

With eqs.(19) and (22), we calculate the structure functions for the transmitted flux fluctuations of the Keck data. A typical result is plotted in Fig. 6, which is given by the Keck data in redshift range $z = 2.50 \pm 0.1$ for all QSOs. The error bars are the maximum and minimum of bootstrap resampling. It is well known that the higher order correlation functions for large scale structure samples have larger error than the 2-point correlation function. However, even for the 8th order statistic $\ln S_j^8/(S_j^2)^4$, the error bars are not much larger than that of the power spectrum, i.e., the second order statistics P_j^u. The structure functions are a very stable statistical quantity because the structure functions are a ratio between S_j^{2n} and $(S_j^2)^n$, which reduces the effect caused by high spikes.

Fig. 6 shows that, for a given n, $\ln S_j^{2n}/(S_j^2)^n$ increases with scale j, and therefore, the intermittent exponent ζ is non-zero and negative [eq.(22)]. The distribution of the transmitted flux fluctuations are neither gaussian nor self-similar, but essentially intermittent. At other redshift ranges, the structure functions behave similarly. This conclusion was already found with the local power distribution (Paper I). However, the local power distribution is based on the measures of each individual mode, $\tilde{\epsilon}_{j,l}^F$ and has a large uncertainty. The distribution of local power is not effective for model discrimination. On the other hand, the structure function is calculated by taking an average among modes. Statistically, they are more effective to test models.

This point can be seen with Fig. 7, which plots the structure function $\ln S_j^{2n}/(S_j^2)^n$ of the transmitted flux fluctuations of the simulation samples for the LCDM and WDM models in redshift range $z = 2.50 \pm 0.1$. The error bars are the maximum and minimum of bootstrap resampling. As a comparison, the structure functions of the Keck data are shown in each panel too. We can see from Fig. 7 that the structure functions of the LCDM and WDM models show intermittent behavior. However, the j-dependence of the structure functions of either the LCDM or the WDM models is clearly different from the Keck data. For the simulation samples, the slope is steeper than the Keck data.

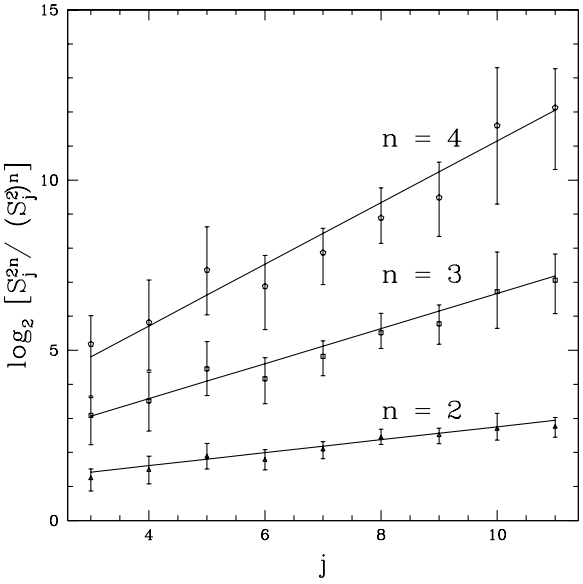

Fig. 6.— $\log_2[S_j^{2n}/(S_j^2)^n]$ vs. j with n=2, 3, 4 for Keck samples in the redshift range $z = 2.5 \pm 0.1$. The error bars are given by the maximum and minimum of bootstrap resampling. The wavenumber for scale j is $k = 0.4 \times 2^{j-11}$ km^{-1} s.

This result shows that the intermittent behavior cannot be measured by any individual high order moment or correlation function, but must be measured by the scale- and n-dependencies of the ratio between the moments.

It is also interesting to point out that the structure functions on small scales $j = 9$, 10, and 11 ($k = 0.1, 0.2$ and 0.4 km^{-1} s) are larger for smaller mass m_W. The structure functions of $m_W = 300$ eV are always the largest one compared to the other models. This is because the WDM model with smaller mass m_W, or longer free-streaming length R_f, lacks power on small scales. The density fluctuations on those small scales mainly originate from the nonlinear process of transferring power from large to small scales (Suto & Sasaki 1991). On the other hand, the structure function $\ln S_j^{2n}/(S_j^2)^n$ is the 2n-th moment S^{2n} normalized by the power S^2, and hence, essentially measures the fraction of density fluctuations which undergoes a nonlinear evolution due to transfer of power. Therefore, smaller m_W leads to a stronger intermittency on scales less than R_f.

Figs. 6 and 7 show that the relations of

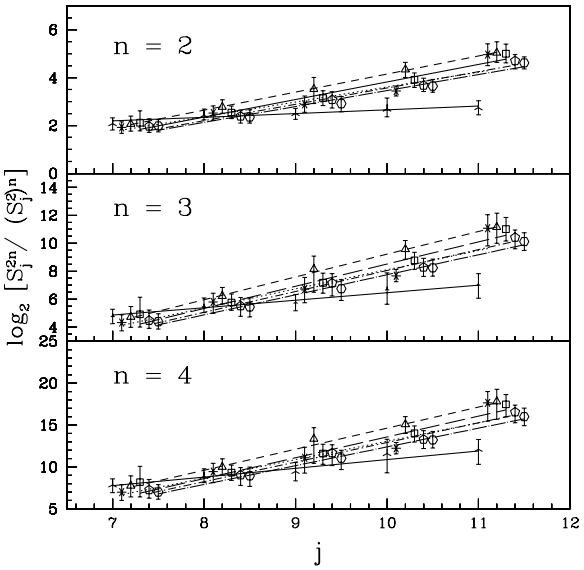

Fig. 7.— $\log_2[S_j^{2n}/(S_j^2)^n]$ vs. j for the models of the LCDM (star) and WDM m_W= 1000 (hexagon), 800 (pentagon), 600 (square) and 300 (triangle) eV in the redshift range $z = 2.5 \pm 0.1$, and $n = 2$, 3 and 4. For comparison, the result for Keck data(vertex with three legs) is also plotted. The error bars are given by the maximum and minimum of bootstrap resampling. For clarity, the points for simulation samples are shifted horizontally to the right from the corresponding j. The wavenumber for scale j is $k = 0.4 \times 2^{j-11}$ km^{-1} s.

$\ln S_j^{2n}/(S_j^2)^n$ vs. j for all models and Keck data can be very well fitted by a line. That is, the intermittent exponent ζ, which is the slope of the fitting line, is a constant in the scale range from $j = 5$ to 11 [eq.(22)], i.e. from $k = 0.006$ to 0.4 km^{-1} s.

6.2. n-dependence of the intermittent exponent

We now turn to the n-dependence of the structure function and intermittent exponent. From eq.(22), we have

$$\zeta(n) = -\frac{1}{j} \ln_2 \frac{S_j^{2n}}{(S_j^2)^n} + \text{const}, \qquad (25)$$

or

$$\zeta(n) - \zeta(1) = -\frac{1}{j} \ln_2 \frac{S_j^{2n}}{(S_j^2)^n}, \qquad (26)$$

For a given j, the n-dependence of $\zeta(n)$ is given by $\ln_2 S_j^{2n}/(S_j^2)^n$ vs. n.

Fig. 8 presents $\ln_2 S_j^{2n}/(S_j^2)^n$ vs. n for the Keck data in the redshift range $z = 2.50 \pm 0.1$. For a gaussian field, the n-dependence of $\ln_2 S_j^{2n}/(S_j^2)^n$ is given by eq.(7), i.e. $\ln_2(2n-1)!!$, which is also plotted in Fig. 8. The figure shows that the difference between the Keck data and a gaussian field is greatest at small scales.

More interesting is to fit the observed n-dependence of $\ln_2 S_j^{2n}/(S_j^2)^n$ with

$$\ln_2 \frac{S_j^{2n}}{(S_j^2)^n} \propto n^\alpha (n-1). \qquad (27)$$

The motivation is simple, as $\alpha = 0$ corresponds to hierarchical clustering [eq.(12)], and $\alpha = 1$ to a lognormal field [eq.(15)]. Fig. 8 shows that the best fit of α for the Keck data is about 0.3 on scales $j = 8$ and 9 ($k = 0.05$ and 0.1 km^{-1} s), but $\alpha \simeq 0.5$ or higher on scales $j = 10$ and 11 ($k = 0.2$ and 0.4 km^{-1} s). This indicates that the transmitted flux is closer to a lognormal field on small scales. In other words, on scales for which the intermittency has been fully developed, the transmitted flux field can be modeled by a lognormal field. This may be the reason that lognormal models of Lyα forests match very well with observations not only at second and lower order statistics of Lyα forests Bi & Davidsen, 1997), but also with higher order behavior, like the scale-scale correlations (Feng & Fang 2000).

Figs. 9 and 10 are, respectively, the $\ln_2 S_j^{2n}/(S_j^2)^n$ vs. n for the LCDM model and the WDM models with $m_W = 300$ eV. They are significantly different from a gaussian field. This is consistent with the CDFs results (§4.2). The best fit for α is always about 0.2, regardless of scale. For the WDM models with other mass m_W, the results are similar to Figs. 9 and 10. That is, the intermittency of the simulation samples is approximately that of hierarchical clustering, i.e., a mono-fractal distribution.

Thus, one may conclude that the intermittency of the simulation samples is different from those of the Keck data not only quantitatively, but also qualitative. The former is scale-independent, and close to a hierarchical clustering, while the later is close to a lognormal field on small scales.

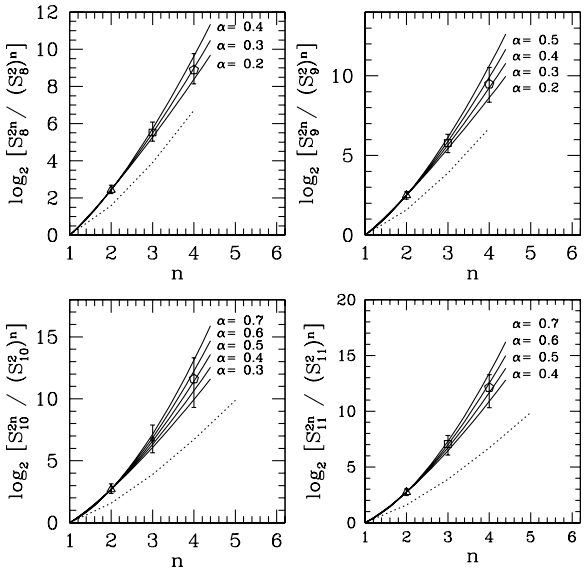

Fig. 8.— $\log_2[S_j^{2n}/(S_j^2)^n]$ vs. n for $j = 8, 9, 10$ and 11 for the Keck data in the redshift range $z = 2.50 \pm 0.1$. The error bars are given by bootstrap resampling. The fitting curves are $n^\alpha(n-1)$. The dotted curves are for gaussian field, i.e. $\log_2[S_j^{2n}/(S_j^2)^n] = \log_2(2n-1)!!$. The wavenumber for scale j is $k = 0.4 \times 2^{j-11}$ km^{-1} s.

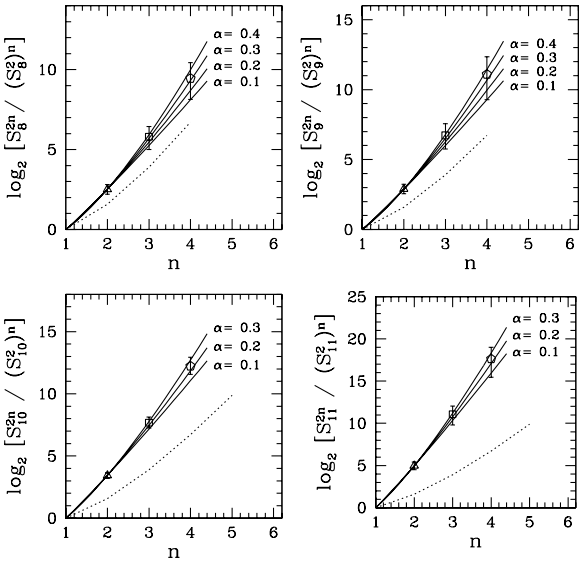

Fig. 9.— $\log_2[S_j^{2n}/(S_j^2)^n]$ vs. n for $j = 8, 9, 10$ and 11 for the simulation samples of the LCDM in the redshift range $z = 2.50 \pm 0.1$. The error bars are given by the maximum and minimum of bootstrap resampling. The fitting curves are $n^\alpha(n-1)$. The dotted curves are for gaussian field, i.e. $\log_2[S_j^{2n}/(S_j^2)^n] = \log_2(2n-1)!!$. The wavenumber for scale j is $k = 0.4 \times 2^{j-11}$ km^{-1} s.

6.3. Redshift-dependence of intermittent exponent

In the last two subsections, only redshift $z = 2.4$ to 2.6 is considered. For other redshift bins, the result is about the same as $z = 2.4$ to 2.6. The ζ against redshift z for $n = 2$, 3 and 4 is shown in Fig. 11. The error bars are from the least squares fitting [eq.(25)].

In all redshift ranges, the value of $|\zeta|$ for the Keck data is found to be substantially and systematically lower than that of the LCDM and WDM models. This can directly be seen from with Fig. 7. This is also consistent with Figs. 8-10. It is interesting that either for the Keck data or the models, the intermittent exponents are almost independent of redshifts in the range $z = 2$ to 4. This is very different from both the observation and theory of massive halos. Collapsed halos with mass on the order of galaxies and clusters undergo a significant evolution in the redshift range from 4 to 2.

The difference between the statistics of the Lyα forests and massive halos is probably due to the fact that the QSO's transmitted flux is given mainly by the absorption of baryonic matter outside of the collapsed massive halos, i.e., the weakly clustered area. Collapsed halos correspond to the saturated absorption in the transmitted flux for which the S/N generally is low. Therefore, the Lyα forest does not contain information on the details of the massive halos.

Fig. 11 also shows that the intermittent exponents of the LCDM and WDM models with $m_W = 300$ eV are about the same. This is also different from massive halos, for which the LCDM and WDM models predict different mass density profiles and number of substructures.

We have simulated the intermittent formation at high redshift. The results show that in the area outside of the collapsed halos, the intermittency is already well developed at redshift $z \sim 5$, and does not increase much for $z \leq 5$. Therefore, intermittency is probably the earliest developed nonlinear feature formed during the evolution from the lin-

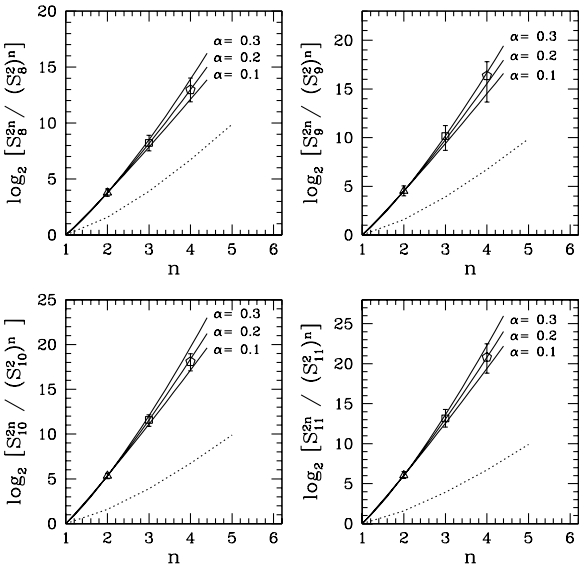

Fig. 10.— $\log_2[S_j^{2n}/(S_j^2)^n]$ vs. n for $j = 8, 9, 10$ and 11 for the simulation samples of the WDM $m_W = 300$ eV. in the redshift range $z = 2.50 \pm 0.1$. The error bars are given by bootstrap resampling. The fitting curves are $n^\alpha(n-1)$. The dotted curves are for gaussian field, i.e. $\log_2[S_j^{2n}/(S_j^2)^n] = \log_2(2n-1)!!$. The wavenumber for scale j is $k = 0.4 \times 2^{j-11}$ km^{-1} s.

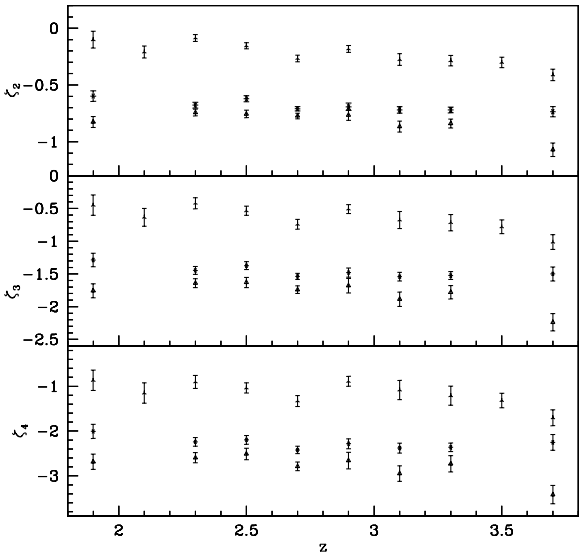

Fig. 11.— ζ_n vs. z, with n=2, 3, 4 for the Keck data and the LCDM (a), and WDM with $m_W = 300$ eV. The error bars are from the least squares fitting.

ear to the nonlinear regimes.

6.4. The effect of noise

In the above calculations, we generally take the parameter $f = 1$, i.e., drop modes with $S/N \leq 1$. The effect of noise on the statistical result can be estimated by the f-dependence, as large f is equal to adding large noise to the simulation samples, but still taking $f = 1$. In Paper I, we showed that the power spectrum P_j^u is almost f-independent when $f = 1$ to 5.

Fig. 12 shows $\ln S_j^{2n}/(S^2)^n$ vs. j for the LCDM model when the noise and f are treated as follows: 1.) sample without adding noise, and $f = 0$; 2.) sample without adding noise and $f = 3$; 3.) sample with adding noise and $f = 3$. Fig. 12 shows that the effect of noise and f should be considered only on the smaller scale $j = 11$, and can be ignored on all other scales.

Fig. 13 is similar to Fig. 10, but with added noise and taking $f = 3$. Similar to Fig. 12, the effect of noise and f on α should be considered only on the smallest scale $j = 11$ and gives α of about 0.45. Even in this case, the simulation samples are still significantly different from the Keck data. Therefore, one can conclude that all results of §6.1 to 6.3 are not very sensitive to noise.

7. Discussions and conclusions

7.1. Model-discriminator of nonlinear regime

In the Paper I, we showed that in the nonlinear regime, the cosmic mass field is intermittent and the power spectrum will on longer be a critical discriminator among models of structure formation. In this paper, we show that for an intermittent field, the structure functions and intermittent exponent are the critical discriminators for models of structure formation. This discriminator can be employed not only to distinguish gaussian and non-gaussian fields, but to detect the *type* of the non-gaussianity. With the n- j- and z-dependence of the structure functions and the intermittent exponent, we are able to distinguish between various nonlinearly evolved fields in detail. That is, the intermittent exponent provides both qualitative and quantitative measures of the cosmic mass and velocity fields from the linear to nonlinear regimes

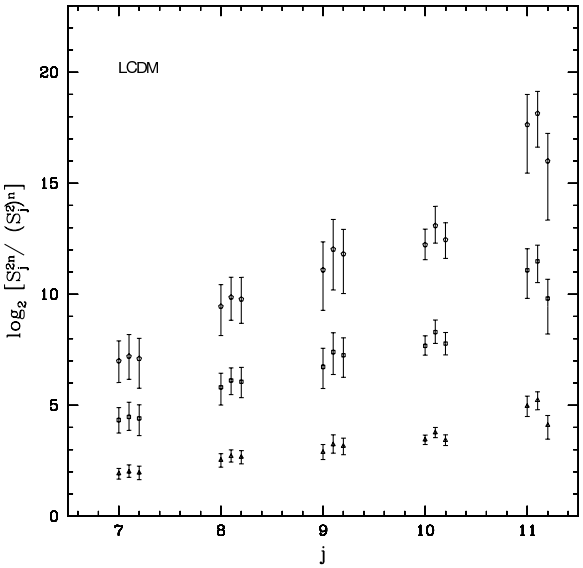

Fig. 12.— $\log_2 S_j^{2n}/(S^2)^n$ vs. j for simulation sample of the LCDM. The noise and f are treated by the following ways: 1.) sample without adding noise, and $f = 0$ (triangle), 2.) sample without adding noise and $f = 3$ (square), 3.) sample with adding noise and $f = 3$ (pentagon). For clarity, the points for 2.) and 3.) are shifted horizontally to right from the corresponding j. The wavenumber for scale j is $k = 0.4 \times 2^{j-11}$ km^{-1} s.

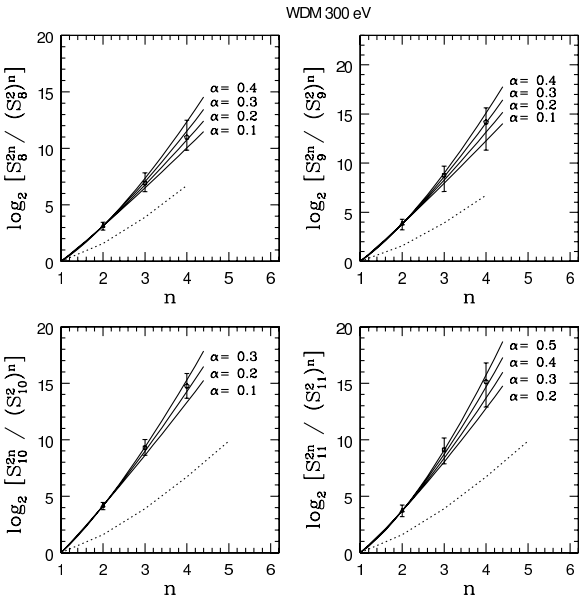

Fig. 13.— The same as Fig. 10, but the sample is added with noise and f is taken to be 3.

and from large to small scales.

We show that the distribution of the transmitted flux fluctuations of the QSO's Lyα forests is intermittent and closer to a lognormal field on small scales. Obviously, this conclusion is important in order to understand the dynamics of the clustering evolution of baryonic matter. It will be interesting to study when this feature formed, and whether the intermittency on scales less than $j = 11$ ($k = 0.4$ km^{-1} s) is closer to a lognormal field. These problems can be studied with samples at higher redshift and higher S/N than the one used in this work.

Using intermittent features, even "weakly" clustered samples, such as QSO's Lyα absorption spectrum, can play an important role for testing structure formation dynamics in the nonlinear regime. It is also important to detect the intermittency of galaxy distributions, as the transmitted flux of Lyα cannot provide information of highly collapsed regions in the cosmic mass field. Note that from the definition of the structure function eq.(1), the intermittent exponent is bias-free if the galaxy bias is linear, i.e. $\rho_{galaxy} = b\rho_{dark\ matter}$.

7.2. Problems with the LCDM and WDM samples

Although the pseudo-hydro simulation samples for the LCDM and WDM models are good in agreement with the Keck data in terms of the power spectrum, PDF and CDF of the transmission flux fluctuations, they are significantly and systematically inconsistent with the intermittent features of the Keck data. Specifically, 1.) the structure functions of the simulation samples are larger than that of Keck data on scales less than $k = 0.1$ km^{-1} s; 2.) the intermittent exponents of the simulation samples are more negative than that of Keck data on all redshifts considered; 3.) the n-dependence of the intermittent exponent of simulation samples are close to the intermittency of hierarchical clustering on all scales, while the Keck data are close to a lognormal field on small scales. That is, the model-predicted intermittency is quantitatively and qualitatively different from the observed results.

This is probably the first result to reveal the deviation of the popular dark model LCDM model

from the Lyα forest observations. However, we should be very careful in reaching conclusions ruling out the relevant dark matter models. For a linear gaussian field, all statistics can be determined by power spectrum with given dark matter parameters. However, intermittency arises from the nonlinear evolution and depends not only on the cosmological parameters, but also on 1.) dynamical assumptions of the relation between the IGM and underlying dark matter field and 2.) parameters used for simulation.

For instance, the lognormal model of Lyα forests (Bi & Davidsen 1997, Feng & Fang 2000) assumes phenomenologically that the nonlinear field of baryonic matter is given by a lognormal transformation of the underlying mass field in linear regime. The sample given by this dynamical assumption can certainly fit with a lognormal PDF of the Lyα transmitted flux.

In the pseudo hydro simulation, the density of baryonic matter in each pixel is assigned according to the dark matter density at that pixel. This is equal to phenomenologically assuming that the statistical property of the baryonic matter is determined by the underlying mass field. This assumption is reasonable in terms of second and lower order statistics. However, it may not be correct in the context of intermittency. That is, although baryonic matter can be considered as a passive component in the system consisting of dark matter and baryonic matter, the statistical properties of the passive component can decouple from the underlying mass field during the nonlinear evolution (Shraiman & Siggia 2000). For instance, a diffused passive substance can exhibit intermittency, even when the underlying mass field is gaussian (Kraichnan, 1994). This is due to the nonlinear evolution of this two component system.

Moreover, the parameters of simulation may also cause uncertainty in measuring the intermittency. In the paper I, we studied the effect of the sample size on the power spectrum. When the characteristic spacing between high spikes (long tail events) exceed the spatial size of samples, the spatial averages cease to coincide with ensemble averages. As a consequence, the mean power of the transmission fluctuations is concentrated in rare but large spikes while the other modes have low power, or are even inactive. We showed that on scales less than $k \simeq 0.10$ km^{-1} s, 50% or more of the power is contributed by the top 5% modes for unnormalized power spectrum, and 1% modes for the locally-normalized power spectrum. Therefore, before making conclusions about the dark matter parameters, we should study whether the deviation is caused by the dynamical assumptions on the relation between the IGM and dark matter. We should also study the effects of simulation parameters (size, resolution etc) on intermittency.

Nevertheless, the current result is strong enough to conclude that all theory and models on the dynamics of nonlinear evolution of the cosmic mass and velocity fields must be examined with their predictions of intermittency. For models which are almost degenerate in the linear regime, the tests with intermittency in nonlinear regime are crucial.

Finally, we should mention that the dynamical evolution of cosmic clustering was found to be able to sketch by the stochastic-force-driven Burgers' equation (Berera & Fang 1994; Jones 1999), or the so-called KPZ equation (Kardar, Parisi & Zhang 1986; Barabási & Stanley 1995). These equations are typical of dynamical models which lead to intermittency (e.g. Polyakov, 1995; E, et al 1997; Balkovsky et al. 1997). These examples clearly illustrate that intermittency is a basic property of the nonlinearly evolved cosmic mass field. Hence, we strongly believe that intermittency is a window to the dynamical evolution of cosmic nonlinear clustering. Knowledge of intermittency may ultimately lead to a better understanding of the still intractable problem of galaxy formation.

LLF acknowledges support from the National Science Foundation of China (NSFC) and National Key Basic Research Science Foundation. PJ also acknowledges the support of the Dean's Dissertation Fellowship at the University of Arizona. We also thank Stephane Colombi for some very insightful comments that improved this manuscript.

REFERENCES

Balkovsky, E., Falkovich, G., Kolokolov, I. & Lebedev, V. 1997, Phys. Rev. Lett. 78, 1452

Barabási, A.L. & Stanley, H.E. 1995, *Fractal Concepts in Surface Growth*, (Cambridge Univ. Press)

Batchelor, G.K. & Townsend, A.A., 1949, Proc. R. Soc. Lond. A 199, 238

Berera, A. & Fang, L.Z. 1994, Phys. Rev. Lett., 72, 458

Bi, H.G & Davidsen, A. F. 1997, ApJ, 479, 523.

Burkert, A., 1995, ApJ, 477, L25

Daubechies I. 1992, *Ten Lectures on Wavelets* (Philadelphia: SIAM)

E., W., Khanin, K., Mazel, A. & Sinai, Y. 1997, Phys. Rev. Lett. 78, 1904

Fang, L.Z. & Feng, L.L. 2000, ApJ, 539, 5

Fang, L.Z. & Thews, R. 1998, *Wavelet in Physics* (Singapore: World Scientific)

Feng, L.L. & Fang, L.Z. 2000, ApJ, 535, 519

Feng, L.L. Pando, J. & Fang, L.Z. 2001, ApJ, 555, 74

Flores, R., & Primack, J.R., 1994, ApJ, 427, L1

Frisch, U. 1995, *Turbulence*, (Cambridge Univ. Press)

Jamkhedkar, P., Zhan, H. & Fang, L.Z. 2000, ApJ, 543, L1

Jamkhedkar, P., Bi, H.G. & Fang, L.Z. 2001, ApJ, 561, 94

Jamkhedkar, P., Feng, L.L., Zheng, W., Kirkman, D., Tytler, D. & Fang, L.Z. 2002,

Jing, Y.P. & Suto, Y. 2000, ApJ, 529, L69

Jones, B.T., 1999, MNRAS, 307, 376

Kardar, M, Parisi, G & Zhang, Y.C. 1986, Phys. Rev. Lett. 56, 342.

Kirkman, D. & Tytler, D. 1997, ApJ, 484, 672

Kraichnan, R.H. 1994, Phys. Rev. Lett. 72, 1016

Mallat, S.G. 1989a, IEEE Trans, on PAMI, 11, 674

Mallat, S.G. 1989b, Trans. Am. Math. Soc. 315, 69

Meyer, Y. 1992, *Wavelets and Operators*, (Cambridge Press, New York).

Pando, J & Fang, L.Z. 1996, ApJ, 459, 1

Pando, J. & Fang, L.Z., 1998, Phys. Rev. E57, 3593

Peebles, P. J. E., 1980, *The large scale structure of the universe*, (Princeton University Press)

Polyakov, A.M. 1995, Phys. Rev. E52 6183

Shraiman B.I. & Siggia, E.D. 2000, Nature, 405, 8

Soneira, R. M.; Peebles, P. J. E. 1977, ApJ, 211, 1

Suto, Y., & Sasaki, M. 1991, Phys. Rev. Lett., 66, 264

Vanmarcke, E.H. 1983, *Random Fields, analysis and synthesis*, (MIT Press, 1983).

White, S.D.M. 1979, MNRAS, 186, 145.

Yang, X.H., Feng, L.L., Chu, Y.Q. & Fang, L.Z., 2001a, ApJ, 553, 1

Yang, X.H., Feng, L.L., Chu, Y.Q. & Fang, L.Z., 2001b, ApJ, 560, 549.

Zhan, H., Jamkhedkar, P. & Fang, L.Z. 2001, ApJ, 555, 58

This 2-column preprint was prepared with the AAS LaTeX macros v5.0.